PCCP

Accepted Manuscript

ROYAL SOCIETY OF CHEMISTRY

www.rsc.org/pccp

Figure captions

Fig. 1. Comparison of electrochemical performance of 2032-type coin cells according to presence of VC in electrolyte; (a) cycling performance of the cell at 60°C at the 1C-rate, (b) charge-discharge performance of the NCM523 with and without VC in electrolyte.

Fig. 2. Electrochemical impedance spectroscopy results of each cell after 1^{st} and 30^{th} cycle; (a) cycled at 60°C without VC, (b) cycled at 60°C with VC.

Fig. 3. DSC measurement results of; (a) the electrolyte solution of 1.15M $LiPF_6$ in EC/EMC (3/7, volume ratio) with and without 2wt.% of VC's addition and (b) cathode materials collected from each 2032-type coin cell after 60cycles with 1C-rate at 60°C.

Fig. 4. C1s XPS results of each sample according to sputtering time; (a) NCM523 without VC, (b) NCM622 without VC, (c) NCM523 with VC, (d) NCM622 with VC.

Fig. 5. Atomic ratio profile of each element consisting of surface layer on cathode; (a) NCM622 without VC, (b) NCM622 with VC.

Fig. 6. F1s XPS results of each sample according to sputtering time; (a) NCM523 without VC, (b) NCM622 without VC, (c) NCM523 with VC, (d) NCM622 with VC.

Fig. 7. Schematic illustration of reduction process of EMC and its resultant products.

Fig. 8. O1s XPS results of each sample according to sputtering time; (a) NCM523 without VC, (b) NCM622 without VC, (c) NCM523 with VC, (d) NCM622 with VC.

Fig. 9. Li1s XPS results of each sample according to sputtering time; (a) NCM523 without VC, (b) NCM622 without VC, (c) NCM523 with VC, (d) NCM622 with VC.

Fig. 10. P2p XPS results of each sample according to sputtering time; (a) NCM523 without VC, (b) NCM622 without VC, (c) NCM523 with VC, (d) NCM622 with VC.

Fig. 11. Mn2p XPS results of each sample according to sputtering time; (a) NCM523 without VC, (b) NCM622 without VC, (c) NCM523 with VC, (d) NCM622 with VC, (e) NCM523 pristine electrode, (f) NCM622 pristine electrode.

Fig. 12. Schematic illustrations of postulated formation process of surface protective layer when VC was added to electrolyte.

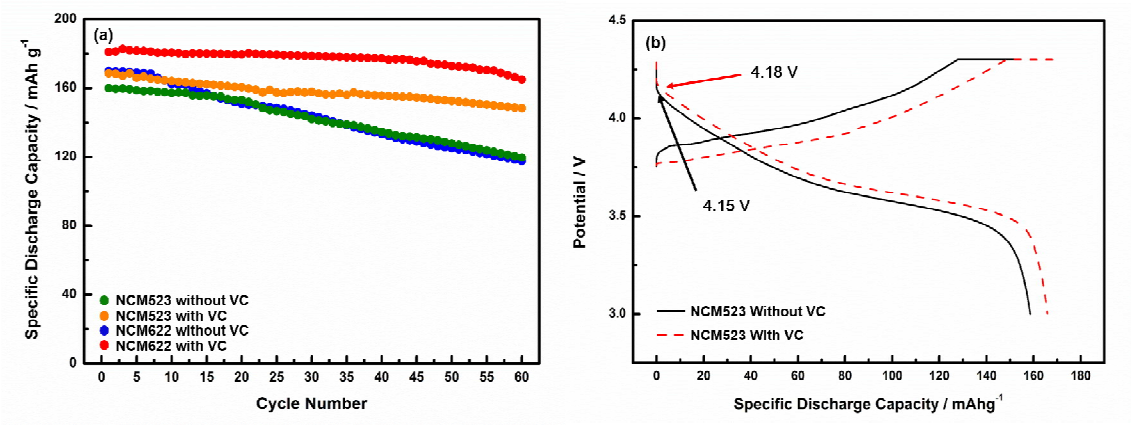

Fig. 1.

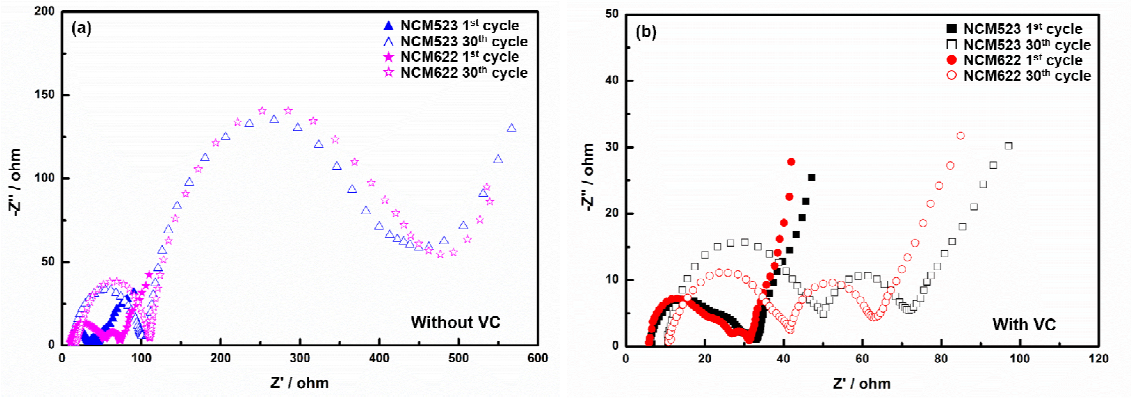

Fig. 2.

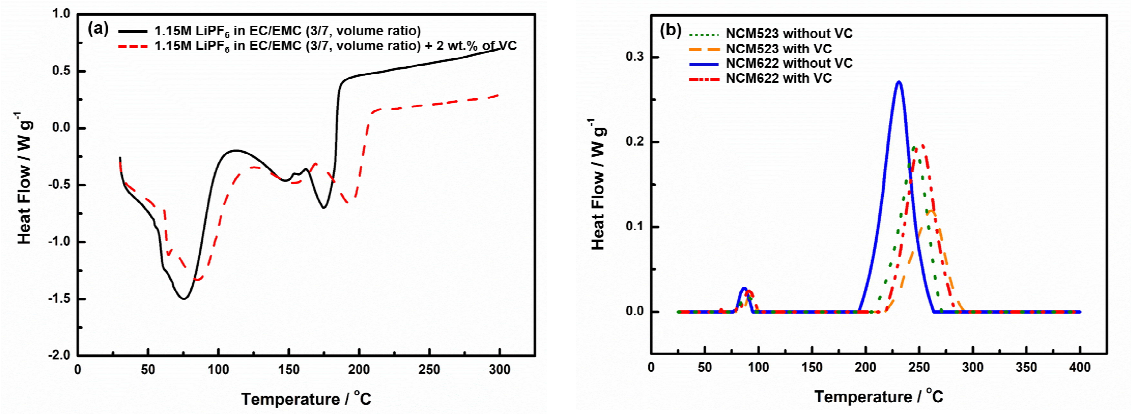

Fig. 3.

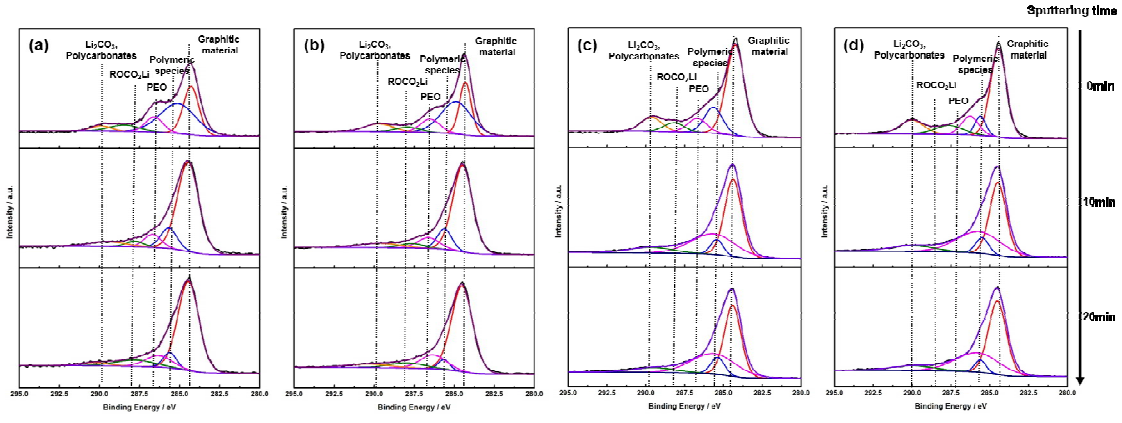

Fig. 4.

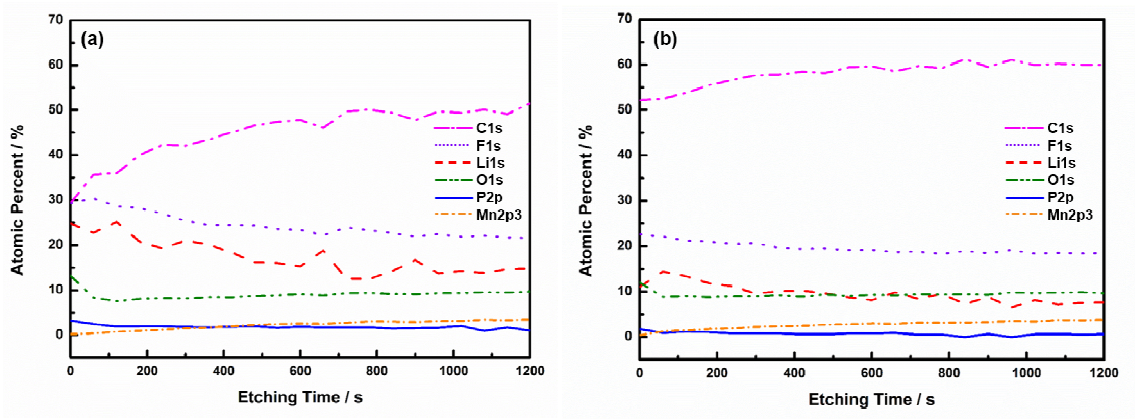

Fig. 5.

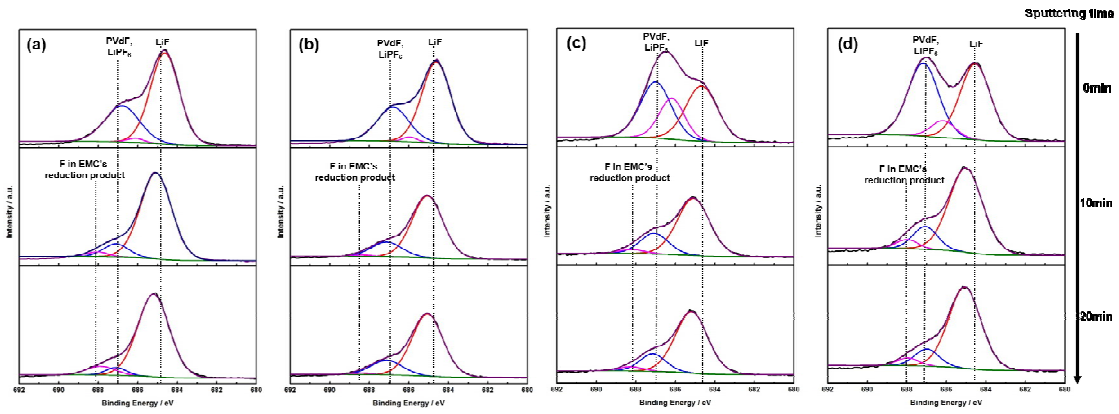

Fig. 6.

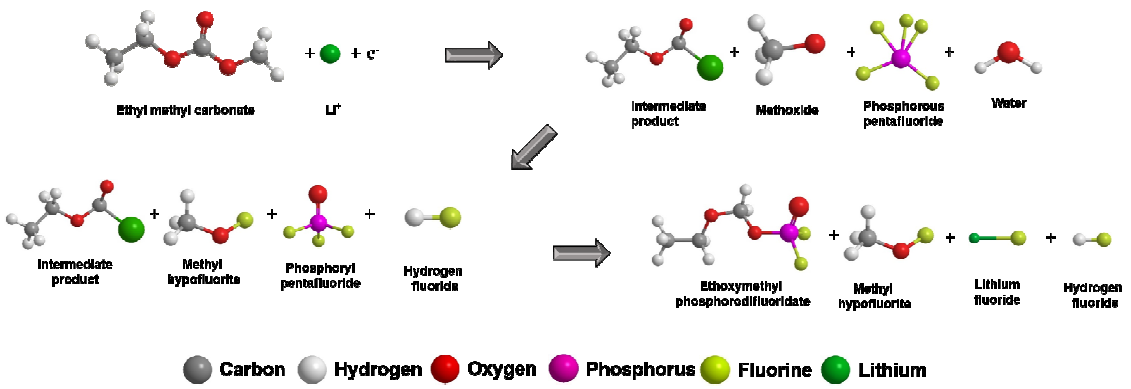

Fig. 7.

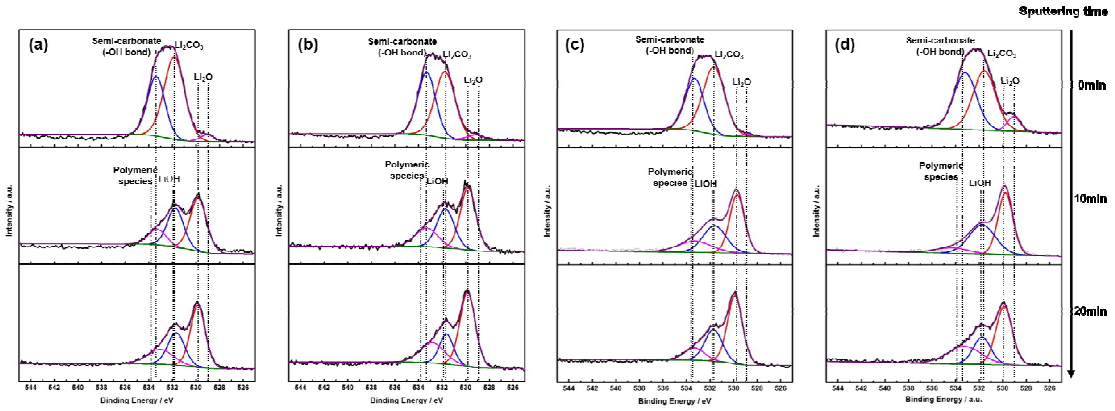

Fig. 8.

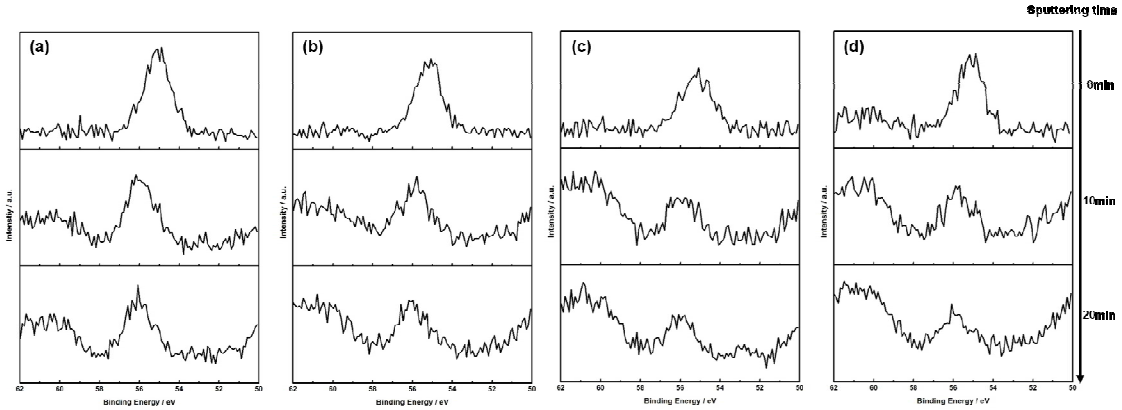

Fig. 9.

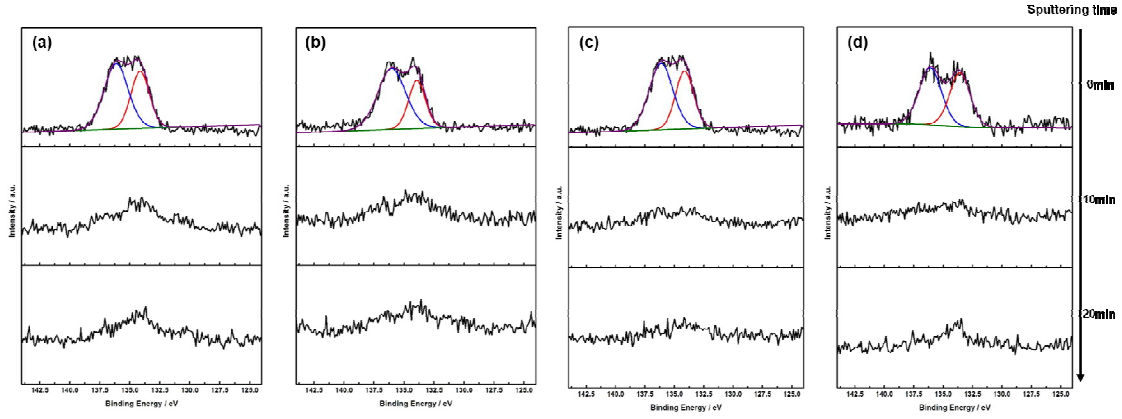

Fig. 10.

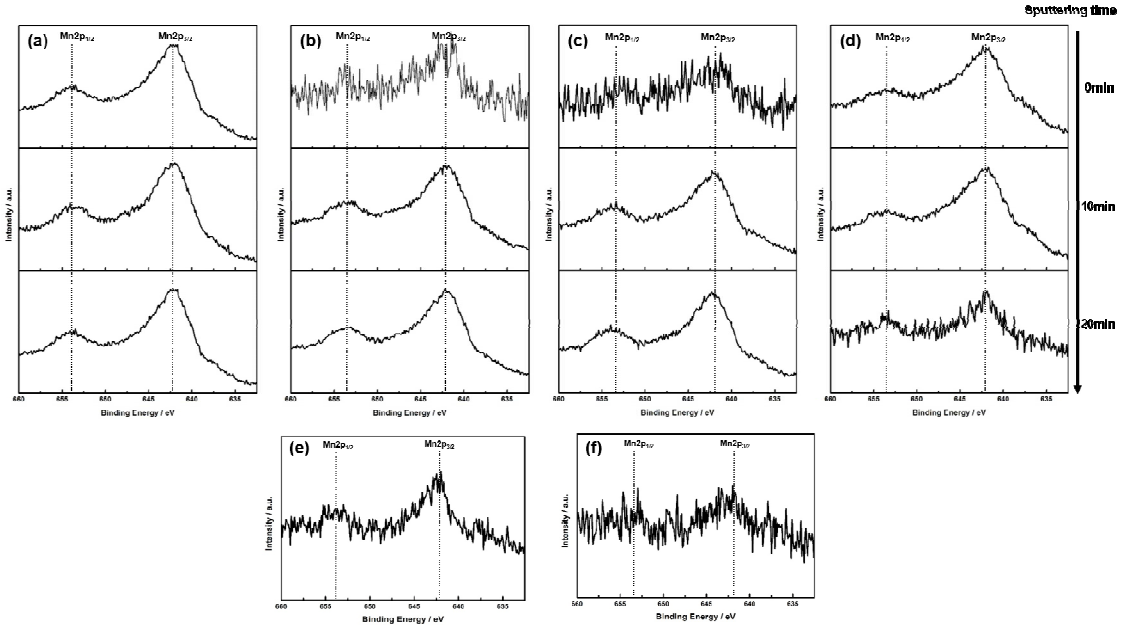

Fig. 11.

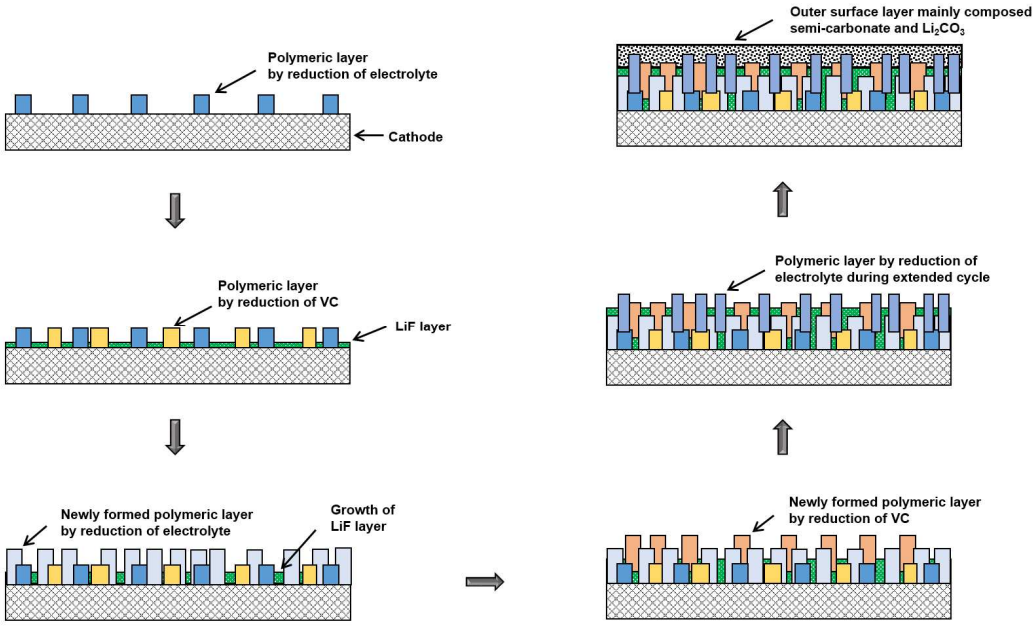

Fig. 12.

Graphical Abstract

[Schematic illustrations of postulated formation process of surface protective layer when VC was added to electrolyte]

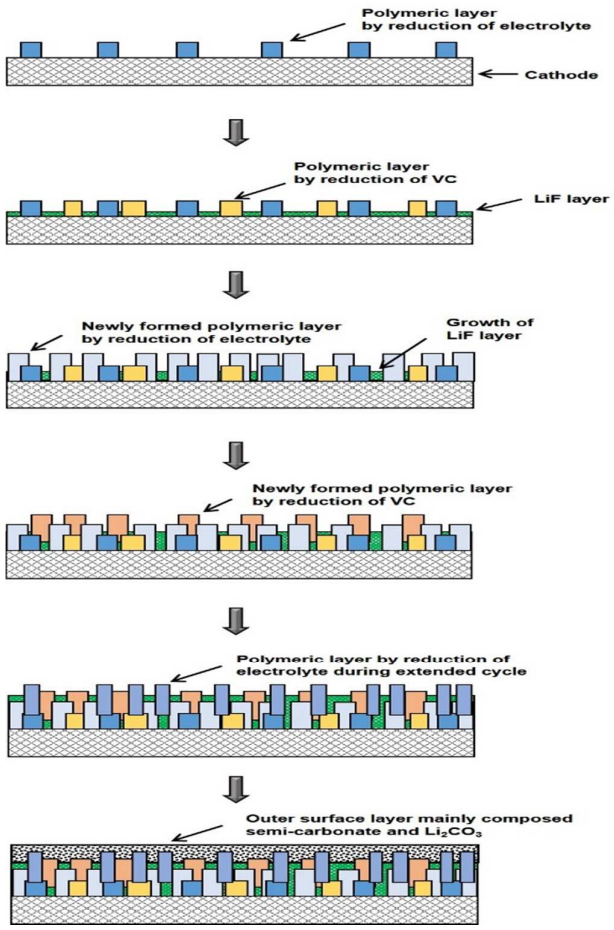

Table 1.

Electrochemical properties of the cells during the cycling at 60°C.

	Reduction Onset Potential	Specific Discharge Capacity at 60th Cycling	Coulombic Efficiency at 60th Cycling	Capacity Retention
NCM523 Without VC	4.15 V	119.6 mAh g^{-1}	96.1 %	74.8 %
NCM523 With VC	4.18 V	148.3 mAh g^{-1}	97.7 %	87.9 %
NCM622 Without VC	4.15 V	117.6 mAh g^{-1}	94.6 %	69.3 %
NCM622 With VC	4.18 V	165.0 mAh g^{-1}	98.3 %	91.2 %

Table 2.

The measured values of respective parameters of electrochemical impedance spectroscopy (EIS) plot.

	NCM523 Without VC		NCM523 With VC		NCM622 Without VC		NCM622 With VC	
	1st cycle	30th cycle	1st cycle	30th cycle	1st cycle	30th cycle	1st cycle	30th cycle
R_{sol}	12.5 Ω	12.2 Ω	4.8 Ω	9.3 Ω	8.9 Ω	18.9 Ω	4.1 Ω	10.3 Ω
R_{film}	22.1 Ω	90.5 Ω	25.8 Ω	42.9 Ω	46.1 Ω	91.7 Ω	23.5 Ω	31.2 Ω
R_{ct}	12.5 Ω	343.2 Ω	8.5 Ω	25.8 Ω	23.3 Ω	368.3Ω	6.2 Ω	22.5 Ω

Table 3.

Assignment of binding energy of each fitted curve of XPS depth profiling for the fully charged cathodes, after 50 cycles at 60°C, without VC additive in the electrolyte.

	0min		10min		20min	
Peak	NCM523	NCM622	NCM523	NCM622	NCM523	NCM622
C1s	284.3 285.1 286.6 288.5 289.9	284.3 284.9 286.5 287.7 289.9	284.5 285.7 286.3 287.9 290.3	284.5 285.6 286.6 287.6 289.6	284.5 285.6 286.3 287.8 290.3	284.5 285.7 286.3 287.9 290.3
O1s	531.8 533.4 529.1	529.2 531.8 533.3	529.8 531.7 533.3	529.8 531.7 533.3	529.8 531.6 532.8	529.8 531.7 533.0
F1s	684.6 686.8 686.1	684.6 686.0 686.8	685.1 687.1 688.1	685.1 687.1 688.3	685.1 687.2 688.4	685.2 687.1 687.9
P2p	134.1 136.1	133.9 136.0	-	-	-	-
Li1s	55.1	55.1	-	-	-	-

Table 4.

Assignment of binding energy of each fitted curve of XPS depth profiling for the fully charged cathodes, after 50 cycles at 60°C, with VC additive in the electrolyte.

	0min		10min		20min	
Peak	NCM523	NCM622	NCM523	NCM622	NCM523	NCM622
C1s	284.2 285.7 286.7 288.2 289.6	284.4 285.6 286.3 287.6 290.0	284.4 285.4 285.7 289.7	284.5 285.5 285.7 290.0	284.4 285.4 285.6 289.5	284.5 285.6 285.8 289.0
O1s	528.8 531.7 533.3	529.1 531.6 533.2	529.7 531.6 533.3	529.9 531.8 533.3	529.8 531.8 534.3	529.9 531.7 533.3
F1s	684.7 686.2 687.0	684.5 686.3 687.2	685.1 687.1 688.2	685.0 687.1 688.0	685.2 687.1 688.3	685.1 687.1 688.0
P2p	134.0 136.0	133.6 136.1	-	-	-	-
Li1s	55.1	55.2	-	-	-	-

Depth profile studies on nickel rich cathode material surfaces after cycling with electrolyte containing vinylene carbonate at elevated temperature

Won Jong Lee, K. Prasanna, Yong Nam Jo, Ki Jae Kim, Hong Shin Kim, Chang Woo Lee*

Department of Chemical Engineering, College of Engineering, Kyung Hee University, 1732 Deogyeong-daero, Gihung, Yongin, Gyeonggi 446-701, South Korea

Abstract

Lithium-ion batteries with vinylene carbonate (VC) in electrolyte exhibit superior electrochemical and thermal behavior at elevated temperature, especially with high Ni content in the cathode material. When VC is added to the electrolyte, polymeric species are formed on the cathode surface by a ring-opening reaction of ethylene carbonate (EC) in the electrolyte and VC, respectively. Through x-ray photoelectron spectroscopy (XPS) depth profiling, we have confirmed that these polymer layers are porous and complementary to each other. XPS results of C1s and O1s show that the outer surface and the inner layer consist of different components. Based on the XPS depth profiling results, we have suggested a reaction mechanism for the formation of a thermally stable layer on the cathode when vinylene carbonate is added to the electrolyte.

Keywords: Vinylene carbonate, High nickel, Surface layer, XPS, Depth profile

*Corresponding author. Tel.: +82-31-201-3825; fax: +82-31-204-8114.

E-mail address: cwlee@khu.ac.kr (Chang Woo Lee).

1. Introduction

Lithium-ion batteries (LIBs) are regarded as the most appropriate energy storage system for electric vehicles (x-EV, x = hybrid, plug-in hybrid, zero-emission) due to their high energy density compared with other battery systems. On the other hand, LIBs for EVs require high capacity and should overcome the safety issues related to thermal runaway during use. Although a cell shows good performance at room temperature, elevated temperatures could cause unexpected side reactions followed by inferior cell performance, overcharging, short circuiting or even explosion. There are several reports about such safety problems, and many groups have focused on investigating the chemistry of the electrode surface in various ways.[1-5] Thus, the importance of exploring and establishing a proper model of the surface chemistry of battery systems is required for the development of improved LIBs.

The solid electrolyte interphase (SEI) layer is known to stabilize the operation of LIBs by suppressing further reactions on the electrode surface.[6-8] Also, it aids in the transport of lithium ions from the electrolyte to the electrode. Therefore, understanding the formation mechanism of the SEI layer is a key aspect of exploring the surface chemistry between the electrode and electrolyte. Through previous studies, many SEI formation or morphology models have been suggested,[9-14] but these mainly focused on anode surfaces. There are, however, no clear models for formation of the SEI layer on the cathode surface.

Vinylene carbonate (VC) has been reported as a successful additive that improves battery performance.[15-18] Recently, VC has attracted attention from researchers for its positive effects on LIB high temperature cycling and storage performance. It is reported that, by adding 2 wt.% VC to an EC based electrolyte, the thermal stability of LIB is improved due to polyvinylene carbonate, which is a reduction product of VC.[19] Also, as the concentration of VC is increased, a higher open circuit voltage is maintained at high temperature (60°C).[20]

In this work, we investigated the formation mechanism of a protective layer on cathodes with high Ni content, i.e., $Li[Ni_{0.5}Co_{0.2}Mn_{0.3}]O_2$ (NCM523) and $Li[Ni_{0.6}Co_{0.2}Mn_{0.2}]O_2$ (NCM622), during

cycling at high temperature in the presence of electrolyte with and without VC. We fixed the concentration of cobalt at 20 % due to its drawbacks like high cost and toxicity. After cycling at high temperature with a 1 C-rate, x-ray photoelectron spectroscopy (XPS) depth profiling was used to characterize the surfaces.

2. Experimental

2.1. Electrode preparation and 2032-type coin cell assembly

The cathode electrode was prepared by the doctor blade coating method. A coating slurry was prepared by mixing the active material (NCM523 and NCM622, Ecopro), polyvinylidene difluoride (PVdF) as a binder, and the conductive agent (denka black) at a ratio of 85:7.5:7.5 by mass in N-methyl pyrrolidone (NMP). Prepared electrode materials were coated on Al foil and dried at room temperature for 24 hours. After drying at room temperature, they were kept in an oven at 120°C for 5 hours under vacuum. A lithium metal foil was employed as the anode. 2032-type coin cells were assembled by sandwiching the separator (Celgard 2340) between the lithium and the prepared cathode with a 1.15M $LiPF_6$ in EC/EMC (3/7, volume ratio) electrolyte with and without 2 wt.% VC. All cells were assembled in a glove box filled with argon gas.

2.1. Characterization

Prepared 2032-type coin cells were cycled at elevated temperature with a cut-off voltage of 3.0-4.3 V (Arbin BT-2000 cycler). Electrochemical impedance spectroscopy (EIS) measurements were performed by a two electrode system applying an AC voltage of 10 mV amplitude over a frequency range from 0.1 Hz to 100 kHz (IVIUM technologies instruments). The cells were left in a delithiated state for 2 hours at room temperature prior to EIS measurements in order to reach equilibrium. For DSC (differential scanning calorimetry) and XPS (X-ray photoelectron spectroscopy) measurements

the prepared cells were disassembled and fully delithiated cathodes were then collected in an argon filled glove box (under 2 ppm of H_2O). The electrolyte solution and collected electrode powders were put in to a high pressure crucible pan (≤15MPa). DSC measurement for powder samples were conducted without washing procedure. The measurements were conducted between the ranges of 25-300°C and 50-400°C with a heating rate of 10°C/min (Mettler Toledo DSC823^e module) for electrolyte solution and electrode powders, respectively. XPS tests were performed using a K-Alpha instrument (Thermo Electron) employing monochromated Al Kα radiation as the X-ray source. The pressure in the chamber was 1.32×10^{-9} bar. The etching of the samples for depth profile measurements was performed with Ar^+ sputtering (2 keV, 20 mins). Obtained results were analyzed using the Thermo Advantage program.

3. Results and discussion

3.1. Electrochemical performance and thermal analysis

The addition of VC to the electrolyte improved the electrochemical behavior of cells at elevated temperature as shown in Fig. 1 (a). The formation cycling were conducted for 5 cycles at room temperature with the current of C/5 as the formation cycles. After the formation cycles, the current rate has been increased to 1C. With bare electrolyte, NCM523 and NCM622 have delivered 159.9 mAh g^{-1} and 169.8 mAh g^{-1} as the first discharge capacity, respectively. Table 1 shows the electrochemical properties of the cells during the cycling at 60^{o}C. After 60 cycles, specific discharge capacities have decreased to 119.6 mAh g^{-1} and 117.6 mAh g^{-1}, respectively, which are 74.8 % and 69.3 % of the initial capacities. The coulombic efficiencies of each cell are also improved as VC is added. Without VC, 96.1 % and 94.6 % of coulombic efficiencies are shown from NCM523 and NCM622, respectively. Meanwhile, the improved coulombic efficiencies are gained as 97.7 % and 98.3 % from NCM523 and NCM622. However, with 2 wt.% VC added to electrolyte, the first discharge capacities of NCM523 and NCM622 were 168.6 mAh g^{-1} and 180.9 mAh g^{-1}, respectively,

and decreased to 148.3 mAh g^{-1} and 165.0 mAh g^{-1} after 60 cycles. About 87.9 % and 91.2 %, respectively, of the initial discharge capacities are maintained, which is greatly enhanced compared with the case where bare electrolyte is used. From Fig. 1 (b), it has been found that the onset charge potential of the samples with and without VC is observed to be similar at 3.75 V, whereas the onset discharge potential for the samples with VC is at 4.18 V and for samples without VC is at 4.15 V. The increase in onset discharge potential of the samples with VC is attributed to the reduction of electrolyte and formation of polymeric species, generally known as SEI layer. It is well known that the initial formation of SEI layer reflects in the initial irreversible capacity but the SEI layer formed due to the presence of VC enables better capacity retention and higher coulombic efficiency with prolonged cycling.

The electrochemical impedance spectroscopy (EIS) results depicted in Fig. 2 demonstrate that the VC's addition can improve the cell's performance at elevated temperature. The intercept of Z' axis is attributed to electrolyte resistance (R_{sol}), the semi-circle at high frequency region is assigned to film resistance (R_{film}) while the second semi-circle at middle frequency corresponds to charge transfer resistance (R_{ct}) which is directly related to interface between electrolyte and electrode, and the 45° line is attributed to diffusion region.[9] Table 2 shows the measured values of respective parameters of EIS plot. Remarkably, the degree of increments of semi-circles is significant when VC is not added to electrolyte. The significant increase of R_{film} can be interpreted as the surface layer is instable at 60°C. More specifically, the surface layer induced by VC's addition has much stronger thermal resistivity against destructive reactions during cycling at high temperature.[21] This feature leads to the protection of electrode at high temperature and it has been reported by several research groups.[19-21] Also, the great increase of R_{ct} has been observed when VC is not added to electrolyte. It means the lithium ions' movement to electrode is hindered in kinetically and electrochemically. Eventually, it is led to the lower capacity of the cell. Our EIS measurement results match to previous reports very well.

In Fig. 3, the thermal stabilizing effect of VC was also confirmed by DSC measurements. Before examining the electrode samples, DSC test on electrolytes with and without VC have been conducted and its results are shown in Fig. 3 (a). Each peak has shifted to higher temperature point and total heat

consumption has decreased from 221.6 Jg^{-1} to 180.7 Jg^{-1} when VC is added. We regard this is due to the thermal stabilization effect of VC as reported previously.[19,22] Also, the same thermal behavior is observed on cathode materials. Fig. 3 (b) describes that the peak points are shifted to a higher temperature range (from 247.1°C to 253.3°C for NCM523 and from 231.2°C to 251.5°C for NCM622), and the heat emission (ΔH) have decreased as well (from 72.3 Jg^{-1} to 62.3 Jg^{-1} for NCM523 and from 85.6 Jg^{-1} to 74.2 Jg^{-1} for NCM622) when VC is added to electrolyte. Interestingly, the positions of the exothermic peaks after the collapse of the surface layer were shifted to a higher temperature range as VC was introduced into the electrolyte (from 91°C to 94.6°C for NCM523 and from 86.6°C to 92.1°C for NCM622); heat emissions decreased as well (from 5.5 Jg^{-1} to 4.2 Jg^{-1} for NCM523 and from 7.8 Jg^{-1} to 5.2 Jg^{-1} for NCM622). These electrochemical and thermal improvements are likely due to the formation of a protective film on the electrode surface,[18,19,21] and the existence of a surface layer induced by the addition of VC to the electrolyte is considered to protect the cathode from abusive cycling at high temperature.

3.2. XPS depth profiling

Fig. 4 shows C1s XPS profiles collected from cathodes after cycling with different electrolytes. Two main peaks are observed at around 284.5 eV and 290.5 eV, which do not relate to the presence of VC. The first one of these peaks can be attributed to graphitic material, and the other at 290.5 eV reflects either Li_2CO_3 or polycarbonates. A shoulder peak at around 286 eV can be assigned to polymeric species. The origin of this peak is still unclear, but is believed to come from hydrocarbon components,[23,24] polymeric species like polymeric ethylene oxide (PEO) [25-27] or ROLi species.[28] Table 3 and 4 show assignment of binding energy of each fitted curve of XPS depth profiling for the fully charged cathodes, after 50 cycles at 60°C, without and with VC additive in the electrolyte, respectively. These carbonates and polymeric species are considered to be from electrolyte reduction. During cycling, EC undergoes a ring-opening reaction. Due to stronger interactions on O···Li-O in lithium alkyl dicarbonate [$(CH_2OCO_2Li)_2$], lithium ethylene di-carbonate is formed on the surface layer more than other species.[29] However, this lithium ethylene di-carbonate is vulnerable to water,

hence it is easily converted to Li_2CO_3 reacting with water.[30,31]

As Ar^+ sputtering proceeds, we have observed remarkable differences on fitted peaks. Fig. 4 (a) and (b) reveal that various peaks are appeared at around 285.6, 286.6, 287.7 and 289.8 eV, which indicate the existence of polymeric species, PEO, $ROCO_2Li$, and Li_2CO_3, respectively when bare electrolyte is used. Compared with those fitted peaks of the very outer surface (0 min of Ar^+ sputtering), there are no significant differences. As depicted in Fig. 4 (c) and (d), however, two peaks are observed in the 285-286 eV range when VC is added. As mentioned above, peaks in this range are due to polymeric species. Thus, unlike the C1s results of the bare electrolyte, addition of VC resulted in new polymeric species on the surface layer. By undergoing robust cycling at high temperature and high C-rate, VC polymerizes through ring-opening reaction and it forms discrete layers on the cathode surface. This layer comes from a reduction product of VC containing a double bond, which is known to help further polymerization on the electrode surface.[32] Due to this polymerization process a unique surface layer is formed on the cathode electrode. In the absence of VC in electrolyte, the unique surface layer is not observed. This phenomena is well clarified by XPS results as well. The two peaks observed at around 286.6 eV are observed at similar points in a deeper part of the surface layer as well. This means the polymerization of VC started in the initial cycles, and the resulting layers remain very stable. These results correspond well with O1s XPS spectra, which will be discussed below. New C–O bonding at around 533.5 eV appeared for the inner layer, which proves the existence of a polymer layer, while $–CO_3$ (532.3 eV) and –OH (533.2 eV) are observed on the very outer surface. These results reveal that polymeric species exist inside the surface layer, but the addition of VC to the electrolyte resulted in the formation of additional polymeric species, which stabilize the surface chemistry of cathodes at high temperature. Fig. 5 shows atomic ratio results and we observed that C1s becomes dominant as Ar^+ sputtering proceeds and results in a larger proportion when VC is used. So, carbon is confirmed as the main component of the surface layer on the cathode.

On the very outer surface of the surface layer, water forms HF by hydrolysis, and the produced HF converts lithium alkyl carbonate to LiF by the equations below.[33]

$$LiPF_6 + H_2O \rightarrow LiF + 2HF + POF_3 \quad (1)$$

$$ROCOOLi + HF \rightarrow LiF + ROH + CO_2(g) \quad (2)$$

LiF produced through these reactions is most commonly found in the surface film. It is known that evolution of LiF mainly happens in the range of 3.8-4.2 V. So, in the last stage of charging, LiF becomes one of the main components of the outer part of the surface layer.[28] However, as depicted in Fig. 6, we have found that the LiF peak stays stable through the whole layer, and this does not depend on the presence of VC in the electrolyte. This means that LiF forms a highly homogeneous layer and is a major component throughout the whole layer. However, the peak at around 687 eV is increased significantly on the outer layer, which indicates the presence of PVdF and $LiPF_6$. So, on the very outer surface, contact between $LiPF_6$ in the electrolyte and the passivation film are reflected in the XPS results. Also, another peak emerged at around 686 eV disappears as Ar^+ sputtering proceeds, while a new peak appears in the range of 687.9-688.25 eV. To explain this phenomenon, we considered the reduction of EMC. By reduction of EMC, a linear organic component with F can be produced and this process is shown in Fig. 7. This organic component undergoes polymerization, and the resultant polymer species is likely the origin of a new peak inside the passive layer. Also, by-products like LiF, HF and CH_3OF are formed as a result of EMC reduction along with the organic component. So, the surface peaks at 686.04-686.18 eV are assigned to by-products of EMC reduction like CH_3OF, which is likely converted to HF in the following reaction.[34]

$$CH_3OF \rightarrow H_2CO + HF \quad (3)$$

Remaining CH_3OF is believed to be indicated in the peak at 687.9 eV.

Fig. 8 shows XPS depth profiling results of O1s. Li_2CO_3 normally is present in the SEI layer formed from EC-based electrolyte. This component is considered as a product of the reaction between semi-carbonate and water or CO_2 gas.[35, 36] As we explore deeper inside the layer, however, the Li_2CO_3 peak decreases, while the Li_2O peak increases. There are two main reasons for the formation of Li_2O. The most widely known reason is that Li_2CO_3 undergoes degradation, and this results in Li_2O formation as indicated in Equation (4) during the Ar^+ sputtering process. Furthermore, it can be

formed by reaction between Li_2CO_3 and lithium ions (Equation (5)).[37] So, Li_2O cannot be regarded as the intrinsic SEI layer.[4,5,26]

$$Li_2CO_3 \rightarrow Li_2O + CO_2\,(g) \quad (4)$$

$$Li_2CO_3 + 2Li^+ + 2e^- \rightarrow 2\,Li_2O + CO \quad (5)$$

However, a recent molecular dynamics study concluded that Li_2O is the primary component of the SEI layer on the lithium metal anode when EC-based electrolyte was used.[36] In order to determine the proper theories for Li_2O in the surface layer on the cathode, further studies are needed. Also, CO_2 gas emitted during formation of Li_2O can react to semi-carbonate on the surface forming Li_2CO_3, and this process is repeated until Ar^+ sputtering is stopped. Another significant difference between the surface layer and the inside layer is the existence of LiOH (peak between 531 eV and 532 eV). Water contamination is a main reason for the formation of LiOH. Water provided by the electrolyte itself and ambient air reacts with Li_2O and form LiOH. Li_2O is supplied continuously by the reaction in Equation (5), so LiOH can continuously accumulate on the electrode surface as well.

As was already mentioned, the shoulder peak at around 286 eV of the C1s XPS depth profiling result corresponds to an attached carbonate oxygen alkyl group. This result agrees well with the XPS profiling result for O1s. Peaks at 531.5 eV and 533.2 eV are a reflection of Li_2CO_3 and semi-carbonate respectively, which significantly decrease in the inner layer. The location of those peaks moved slightly to higher binding energy, and this indicates the transformation of those carbonaceous materials into a more stable state such as polymers. So, polymeric species are more prevalent than other carbonate components in the surface layer.

The different components of the outer and inner layer are also confirmed from the Li1s XPS spectra, as shown in Fig. 9. Before Ar^+ sputtering, a clear peak at 55.5 eV is observed, which seems to be trace lithium from the $LiPF_6$ of electrolyte and Li_2CO_3, which exists at the very outer surface of the surface layer. As Ar^+ sputtering proceeds, polymeric species containing Li appear, as we discussed before, and the existence of those components is demonstrated by an increased intensity of the wing side. Simply, carbon or other elements interfere with the detection of binding energy of pure Li during

XPS tests. P2p XPS spectra which is shown in Fig. 10 can also be explained in the same way. $LiPF_6$ is a main source of phosphate in this system, but with increased XPS depth profiling, its effect on surface layer decreases. So, it is barely detectable well below the surface.

We confirmed that the degree of capacity fading is significant as Ni content increased without VC in the electrolyte from Fig. 1 and Table. 1. Elevated temperature can accelerate capacity fading including aging of active material, structural changes during cycling and also chemical decomposition/dissolution reaction.[38,39] During cycling, the $LiMO_2$ (M=Ni, Co) layered structure cathode acts as an oxygen provider for oxidation reactions followed by formation of a surface layer of $Li_xM_{1-x}O$ (M=Ni, Co) having a rocksalt structure on the bulk layered material.[40] However, not many works have focused on dissolved Mn ions and their contribution to the building up of surface layer. Mn is a key element of maintaining thermal stability of structure, so we curiously explored Mn2p XPS spectra whether Mn participates in formation of surface protective layer on electrode. For spinel structures, it is well known that the electrolyte is attacked by HF, which propagates at elevated temperature,[41] and HF in the electrolyte caused dissolution of Mn, which proceeds through the below Equation (6).[42]

$$2Mn^{3+} \rightarrow Mn^{4+} + Mn^{2+} \qquad (6)$$

Mn^{2+} separated from the electrode structure can be participated into the SEI on the anode, which finally leads to aging acceleration of the cell.[38,42,43]

Fig. 11 shows XPS depth profiling results of Mn2p. The concentration of Mn ions on the surface is comparatively lower than the inner surface. Also, two sharp peaks are observed around 642 eV and 653 eV, which correspond to $Mn2p_{3/2}$ and $Mn2p_{1/2}$ lines, respectively. Analysis of Mn2p spectra is bit tedious due to the overlap with the NiL3M23M25 Auger spectrum.[44,45] With the observed binding energies, it is concluded that Mn ions are mainly in the 4+ charge state, as mentioned in many previous works. For a better understanding, Mn2p XPS spectra of pristine electrodes have been studied as well and the results are shown in Fig. 10 (e) and (f). The binding energies of Mn from different conditions such as different Mn contents in the cathode material, cycling state, and contact

with the electrolyte are barely changed, which means Mn ions stay in the 4+ charge state in all samples. These results do not suggest or demonstrate Mn ion dissolution or its incorporation in the buildup of the surface layer.

3.3. Postulating formation process of surface layer

Based on XPS depth profiling results, we postulated a process of surface layer formation as shown in Fig. 12. EC and VC undergo a reduction process during cycling. The product of the ring-opening reaction of VC contains double bond, so further polymerization occurs. Also, EMC proceeds through a reduction process and produces CH_3OF, which can be converted into HF. LiF is produced by the reactions described in Equation (1) and Equation (2) and is found in the whole surface layer. Lithium products (mainly LiF and LiOH) and electrolyte products accumulate on those layers. As cycling proceeds, these processes are repeated, and, at the very outer surface, a new layer is formed mainly composed of lithium carbonate and semi-carbonate, which have begun transforming to polymeric species.

4. Conclusions

The electrochemical and thermal behavior of a fully delithiated NCM523 and NCM622 electrode with 1.15 M $LiPF_6$ in EC/EMC (3/7, volume ratio) were investigated in the absence and presence of 2 wt.% VC in electrolyte. Addition of VC brought to improvement in electrochemical and thermal behavior of the cell at elevated temperature (60°C). The thermal stabilizing effect of VC was significant as Ni contents increased, and it is due to the formation of a thermally stable layer on the electrode surface. Through XPS depth profiling, it is confirmed that polymeric species, induced by a ring-opening reaction of EC and VC, formed a complementary layer on the electrode surface. XRD depth profiling results prove this layer is different from the surface layer when bare electrolyte is used.

We believe this difference causes the enhanced thermal behavior of the cell. However, further studies should be conducted to more thoroughly understand this behavior. Also, we have confirmed that the outside and the inside of the surface layer consist of different components by XPS depth profiling results of C1s and O1s. However, addition of VC to the electrolyte resulted in a difference in C1s spectra, but not in the spectra of any other components. We could not find any proof of Mn ion participation in the formation of a surface layer during the cycling. With collated XPS depth profiling results, a formation mechanism of a thermally stable surface layer on a cathode surface when VC is added to the electrolyte has been suggested.

Acknowledgments

This work was supported by the IT R&D program of MOTIE (Ministry of Trade, Industry & Energy) / KEIT (Korea Evaluation Institute of Industrial Technology) [10041856].

References

1 RM. Gnanamuthu, K. Prasanna, T. Subburaj, Y. N. Jo and C. W. Lee, Appl. Surf. Sci., 2013, **276**, 433-436

2 Q. Wang, J. Sun, X. Yao and C. Chen, Thermochim. Acta, 2005, **437**, 12-16.

3 H. Jannesaria, M.D. Emamia and C. Ziegler, J. Power Sources, 2011, **196**, 9654-9664.

4 M. Herstedt, M. Stjerndahl, T. Gustafsson and K. Edström, Electrochem. Commun., 2003, **5**, 467-472.

5 M. Herstedt , H. Rensmob, H. Siegbahn and K. Edström, Electrochim. Acta, 2004, **49**, 2351-2359.

6 G.-C. Chung, J. Power Sources, 2002, **104**, 7-12.

7 M. Balasubramanian, H. S. Lee, X. Sun, X. Q. Yang, A. R. Moodenbaugh, J. McBreen, D. A. Fischer and Z. Fu, Electrochem. Solid-State Lett., 2002, **5**, A22-A25.

8 B. Li, M. Xu, T. Li, W. Li and S. Hu, Electrochem. Commun., 2012, **17**, 92-95.

9 D. Aurbach, J. Power Sources, 2000, **89**, 206-218.

10 A. M. Andersson and K. Edström, J. Electrochem. Soc., 2001, **148**, A1100-A1109.

11 K. Edström, Marie Herstedt and D. P. Abraham, J. Power Sources, 2006, **153**, 380-384.

12 E. Peled, D. Golodnitsky and G. Ardel, J. Electrochem. Soc., 1997, **144**, L208-L210.

13 K. Edström, T. Gustafsson and J.O. Thomas, Electrochim. Acta, 2004, **50**, 397-403.

14 I. A. Profatilova, C. Stock, A. Schmitz, S. Passerini and M. Winter, J. Power Sources, 2013, **222**, 140-149.

15 C.-C. Chang, S.-H. Hsu, Y.-F. Jung and C.-H. Yang, J. Power Sources, 2011, **196**, 9605-9611.

16 I. B. Stojkovic, N. D. Cvjeticanin and S. V. Mentus, Electrochem. Commun., 2010, **12**, 371-373.

17 L. Chen, K. Wang and X. Xie, J. Power Sources, 2007, **174**, 538-543.

18 L. Zhao, S. Okada and J.-I. Yamaki, J. Power Sources, 2013, **244**, 369-136.

19 H.-H. Lee, Y.-Y. Wang, C.-C. Wan, M.-H. Yang, H.-C. Wu and D. -T. Shieh, J. Appl. Electrochem., 2005, **35**, 615-623.

20 J. -Y. Eom, I.-H. Jung and J.-H. Lee, J. Power Sources, 2011, **196**, 9810-9814.

21 H. -C. Wu, C.-Y. Su, D.-T. Shieh, M.-H. Yang and N.-L. Wu, Electrochem. Solid-State Lett., 2006, **9**, A537-A541.

22 E. -G. Shim, T. -H. Nam, J. -G. Kim, H.-S. Kim, S.-I. Moon, J. Power Sources, 2007, **172**, 901-907.

23 K. Kanamura, H. Tamura, S. Shiraishi and Z. Takehara, J. Electrochem. Soc., 1997, **144**, 340-347.

24 L. El Ouatani, R. Dedryvère, C. Siret, P. Biensan and D. Gonbeaua, J. Electrochem. Soc., 2009, **156**, A468-A477.

25 D. B.-Tow, E. Peled and L. Burstein, J. Electrochem. Soc., 1999, **146**, 824-832.

26 A. M. Andersson, D. P. Abraham, R. Haasch, S. MacLaren, J. Liu and K. Amine, J. Electrochem. Soc., 2002, **149**, A1358-A1369.

27 A.M. Andersson, A. Henningson, H. Siegbahn, U. Jansson and K. Edström, J. Power Sources, 2003, **119-121**, 522-527.

28 S. Leroy, F. Blanchard, R. Dedryvère, H. Martinez, B. Carré, D. Lemordant and D. Gonbeau, Surf.

Interface Anal., 2005, **37**, 773-781.

29 J.-K. Park, *Principles and Applications of Lithium Secondary Batteries*, Wiley-VCH, Weinheim, 1st edn., 2012, ch. 3, pp. 208.

30 D. Aurbach, Y. E.-Eli, O. Chusid, Y. Carmeli, M. Babai, H. Yamin, Y. Carmeli, M. Babai and H. Yamin, J. Electrochem. Soc., 1994, **141**, 603-611.

31 J.-S. Shin, C.-H. Han, U.-H. Jung, S.-I. Lee, H.-J. Kim and K. Kim, J. Power Sources, 2002, **109**, 47-52.

32Y. Wang, S. Nakamura, K. Tasaki and P. B. Balbuena, J. Am. Chem. Soc., 2002, **124**, 4408-4421.

33 K. Kanamura, H. Tamura, S. Shiraishi and Z. Takehara, Electrochim. Acta, 1995, **40**, 913-921.

34 M. Koi, S. Rozen and E. Appelman, J. Am. Chem. Soc., 1991, **113**, 2648-2651.

35 Y. Wang, S. Nakamura, M. Ue and P. B. Balbuena, J. Am. Chem. Soc., 2001, **123**, 11708-11718.

36 S.-P. Kim, A.C.T. van Duin and V. B. Shenoy, J. Power Sources, 2011, **196**, 8590-8597

37 S. Malmgren, K. Ciosek, M. Hahlin, T. Gustafsson, M. Gorgoi, H. Rensmo and K. Edström, Electrochim. Acta, 2013, **97**, 23-32.

38 M. M. Thackeray, J. Am. Ceram. Soc., 1999, **82**, 3347-54

39 M. Broussely, Ph. Biensan, F. Bonhomme, Ph. Blanchard, S. Herreyre, K. Nechev and R.J. Staniewic, J. Power Sources, 2005, **146**, 90-96.

40 D.P. Abraham, R.D. Twesten, M. Balasubramanian, I. Petrov, J. McBreen and K. Amine, Electrochem. Commun., 2002, **4**, 620-625.

41 S.-T. Myung, K. Izumi, S. Komaba, Y.-K. Sun, H. Yashiro and N. Kumagai, Chem. Mater., 2005, **17**, 3695-3704.

42 G.G. Amatucci, C.N. Schmutz, A. Blyr, C. Sigala, A.S. Gozdz, D. Larcher and J.M. Tarascon, J. Power Source, 1997, **69**, 11-25.

43 A. Blyr, C. Sigala, G. Amatucci, D. Guyornard, Y. Chabre and I.M. Tarascon, J. Electrochem. Soc., 1998, **145**, 194-209.

44 N.V. Kosova, E.T. Devyatkina and V.V. Kaichev, J. Power Sources, 2007, **174**, 965-969.

45 N.V. Kosova, E.T. Devyatkina and V.V. Kaichev, J. Power Sources, 2007, **174**, 735-740.